university of groningen

University Medical Center Groningen

University of Groningen

Dissociation of fast N-2 molecules scattered from different fcc(110) surfaces

Bruning, K.; Heiland, W.; Schlatholter, T.; Wojciechowski, I. A.; Medvedeva, M. B.; Ferleger, V. K.

Published in:
Journal of Chemical Physics

DOI:
10.1063/1.482063

IMPORTANT NOTE: You are advised to consult the publisher's version (publisher's PDF) if you wish to cite from it. Please check the document version below.

Document Version
Publisher's PDF, also known as Version of record

Publication date:
2000

Link to publication in University of Groningen/UMCG research database

Citation for published version (APA):
Bruning, K., Heiland, W., Schlatholter, T., Wojciechowski, I. A., Medvedeva, M. B., & Ferleger, V. K. (2000). Dissociation of fast N-2 molecules scattered from different fcc(110) surfaces. *Journal of Chemical Physics*, *113*(6), 2456-2469. [PII [S0021-9606(00)70930-5]]. https://doi.org/10.1063/1.482063

Copyright
Other than for strictly personal use, it is not permitted to download or to forward/distribute the text or part of it without the consent of the author(s) and/or copyright holder(s), unless the work is under an open content license (like Creative Commons).

The publication may also be distributed here under the terms of Article 25fa of the Dutch Copyright Act, indicated by the “Taverne” license. More information can be found on the University of Groningen website: https://www.rug.nl/library/open-access/self-archiving-pure/taverne-amendment.

Take-down policy
If you believe that this document breaches copyright please contact us providing details, and we will remove access to the work immediately and investigate your claim.

Downloaded from the University of Groningen/UMCG research database (Pure): http://www.rug.nl/research/portal. For technical reasons the number of authors shown on this cover page is limited to 10 maximum.

Download date: 05-05-2023

Dissociation of fast N_2 molecules scattered from different fcc(110) surfaces

K. Brüning, W. Heiland, T. Schlathölter, I. A. Wojciechowski, M. B. Medvedeva, and V. Kh. Ferleger

Citation: J. Chem. Phys. **113**, 2456 (2000); doi: 10.1063/1.482063
View online: https://doi.org/10.1063/1.482063
View Table of Contents: http://aip.scitation.org/toc/jcp/113/6
Published by the American Institute of Physics

Articles you may be interested in

N_2 dissociative adsorption on Ru(0001): The role of energy loss
The Journal of Chemical Physics **115**, 9028 (2001); 10.1063/1.1413746

PHYSICS TODAY
WHITEPAPERS

ADVANCED LIGHT CURE ADHESIVES

Take a closer look at what these environmentally friendly adhesive systems can do

READ NOW

PRESENTED BY
MASTERBOND
ADHESIVES | SEALANTS | COATINGS

Dissociation of fast N_2 molecules scattered from different fcc(110) surfaces

K. Brüning[a] and W. Heiland
Universität Osnabrück, D-49060 Osnabrück, Germany

T. Schlathölter
KVI Atomic Physics, Rijksuniversiteit Groningen, NL-9747AA Groningen, The Netherlands

I. A. Wojciechowski, M. B. Medvedeva, and V. Kh. Ferleger
Arifov Institute of Electronics, Tashkent 700143, Uzbekistan

(Received 23 March 2000; accepted 10 May 2000)

The dissociation of fast nitrogen molecules with kinetic energies ranging from 200 to 2000 eV/atom was studied for grazing collisions with various fcc surfaces. At these energies, the dissociation is caused by vibrational and rotational excitation, the latter being favored for scattering along the surface semichannels. N_2 is chemically inert and interacts mainly elastically with the surfaces. A controversial question is the role of the dynamic screening of the molecular constituents by the bulk electron gas during the dissociation process. Another interesting issue is the dependence of the dissociation probability on the azimuthal scattering angle—the fragmentation is highest for the low indexed direction. We treat both problems, by comparing results obtained from the different surfaces Pd(110), Ag(110), and Pt(110). The experimental data are compared to molecular dynamics simulations based on realistic interaction potentials as obtained from density functional theory calculations. The potentials are improved by adding an explicit dependence of the intramolecular bond strength on the molecule surface distance *z*, which leads to excellent agreement of experiment and simulations. © *2000 American Institute of Physics.* [S0021-9606(00)70930-5]

I. INTRODUCTION

Dissociation dynamics of molecules at surfaces play a crucial role in a variety of fields such as heterogeneous catalysis, environmental chemistry, modification of materials, and erosion of space vehicles. For molecules with translational energies in the range of 10^2-10^4 eV, different dissociation mechanisms have been proposed,[1] e.g., dissociation following resonant neutralization to antibonding molecular states and purely impulsive dissociation. It is well known, that the orientation of the molecule during the interaction with the surface is of considerable importance for several types of interaction processes at hyperthermal energies[2,3] as well as in the keV regime.[4]

In our prior work on H_2^+ and N_2^+ scattered off the (110)- and (111)-faces of palladium under grazing incidence, we could show that parallel to a low-index direction, mainly rotational excitation occurs whereas for high-index scattering, vibrational excitation is the main reason for dissociation.[5–7] In contrast to molecules such as H_2 or O_2, charge transfer processes during the interaction of N_2 with metal surfaces are of minor importance for the dissociation process,[8–10] even though to a small extent electronical excitation due to violent collisions with surface atoms is possible.[11] N_2 is therefore a perfect system for a direct comparison of N_2^+ scattering experiments with purely classical simulations for neutral N_2. In a prior publication we could show that the experimental results on grazing N_2 scattering from Pd(111) can be described qualitatively by classical trajectory (CT) calculations using a density functional theory (DFT) based analytical potential energy surface (PES).[5] So far, these simulations neither reached a satisfying quantitative agreement nor did they succeed in describing the dissociative behavior of N_2 molecules scattered off the more corrugated (110)-faces, especially when choosing low-indexed directions for the incident beam. Motivated by this lack of agreement we try to refine our classical model for the N_2-surface interaction. Henriksen *et al.* in their approach on calculating the interaction PES for nitrogen/rhenium, use a similar model which includes an additional coordinate-dependent parameter reflecting the observed softening of the N–N vibrational frequency when the molecule is adsorbed.[12] This softening is caused by the mutual screening of the molecular constituents by the free metal electrons. Strictly speaking, this model is only valid for systems where the molecular projectile is much slower than the metal electrons' Fermi velocity: $v_{\mathrm{proj}} \ll v_f$. For systems with fast moving molecules, the softening can become a dynamical process, as for the charge state of moving (atomic) ions in matter.[13–15] The molecule–surface interaction time reaches the order of magnitude of the typical time constant of electronic processes, hence, if the velocity of the molecule becomes comparable to the Fermi velocity, the softening can be incomplete. Due to its nonadiabatic character, the term *dynamic* screening[16,17] is justified. Anyway, the dissociation is affected due to lowering the intramolecular binding force.[18] The v_{proj} reached with the primary energies and N_2 in this work are between 4×10^4 and 2×10^5 ms^{-1}, i.e., at least one order of magnitude lower than typical Fermi velocities of several 10^6 ms^{-1} in metals.

[a]Electronic mail: kbuen@uni-osnabrueck.de

 © 2000 American Institute of Physics

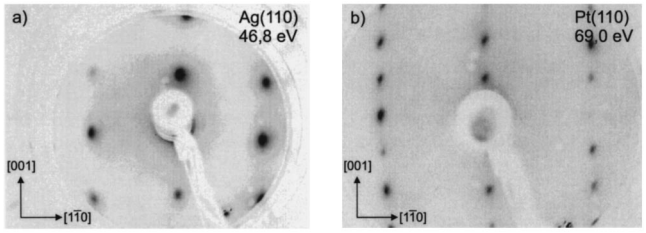

FIG. 1. LEED pattern of the investigated surfaces (inverted). (a) 1×1-structure of Ag(110), which is also found on Pd(110); and (b) 1×2 structure of the Pt(110) surface.

The fcc(110) surfaces provide semichannels of different structure and width. In our earlier work on Pd(110), we found out that the dissociation probability of the scattered molecules increases when going from the $[1\bar{1}2]$ to the $[1\bar{1}1]$ and the $[1\bar{1}0]$ directions, respectively. In the following, we present our energy- and azimuthal-angle resolved studies of N_2 dissociation on Pd(110), Ag(110), and Pt(110) surfaces. We demonstrate that, after determining an ''effective'' softening parameter, the simulations match these experimental results very closely.

II. EXPERIMENT

Details of the experimental setup have been described earlier.[19] The apparatus consists of an ultra-high-vacuum chamber, equipped with a plasma-ion source, an m/q-selection magnet and a time-of-flight (TOF) system. The laboratory scattering angle Θ, the azimuthal orientation of the single crystal target φ, and the TOF-detector ϕ with respect to the incident beam are variable. The TOF spectra are normally taken under specular reflection, i.e., $2\Psi=\Theta$ (Ψ is the glancing angle of incidence) and $\phi=0°$. The angle of acceptance of the TOF detector is 1.2°.

In our investigations, we use Pd(110), Ag(110), and Pt(110), all presenting fcc structures. In contrast to the two other surfaces, Pt(110) is reconstructed at room temperature in the 1×2-*missing-row* pattern.[20] Preparation of the samples is done by the usual cycles of sputtering and annealing, while the cleanliness of the surfaces is probed by ion scattering spectroscopy (ISS).[21,22] The crystallographic directions of the clean surfaces are determined by LEED (Fig. 1) and by azimuthal scans of the specularly reflected ion yield with an absolute accuracy better than $\pm1°$. Focusing and defocusing of the scattered beam, due to the respective crystallographic orientation, sensitively affects its spatial distribution as the visualization via a position sensitive detector (PSD) in Fig. 2 is shown for 2.5 keV Ne^+ particles scattered off a typical fcc(110) surface.

To this end, the intensity of the forward scattered particles—using the small aperture TOF detector—is recorded as a function of the variable azimuth φ, measuring the rotation of the plane of scattering with respect to the $[1\bar{1}0]$ surface direction (Fig. 3). The signal increases significantly along low-index directions. For a particle as He^+, this effect is obviously more pronounced (solid black curve in the plot); but even for the diatomic N_2^+ ion, a strong influence of the surface structure is visible. As determined by the fcc(110) geometry, we find $[1\bar{1}0]$, $[1\bar{1}1]$, and $[1\bar{1}2]$ at $\varphi=0°$, 35.3°, and 54.7°, respectively. A well chosen ''random'' direction can be found under $\varphi=45°$ for all mentioned samples. In order to compare two external conditions, we carry out TOF measurements at different primary energies for the $[1\bar{1}0]$ and the random crystallographic direction, respectively. The TOF spectra presented in Sec. III are converted into energy spectra. The experimental results of our investigations on Pd(111) and Pd(110) have already been published[5,6] but are mentioned here again for comparison with the new simulations.

III. RESULTS

Figure 4(a) shows a typical energy spectrum which is obtained from a TOF measurement. In most cases, each spectrum can be separated into two superimposed peaks, one formed by surviving molecules and the other by single N atoms released by dissociation. The second distribution is broadened and partly extends to values higher than E_0. This indicates a dissociation process in which an energy E_D is released within the center-of-mass-system of the molecule. In the laboratory system, the resulting energy of the constituents can be obtained by a Galilei transformation[19]

$$E_{\mathrm{lab}}=\tfrac{1}{2}E_0+\tfrac{1}{2}E_D\pm\sqrt{E_0E_D}\cos\beta, \tag{3.1}$$

where β is the angle between the molecular axis and the beam direction. Equation (3.1) does not consider any inelastic effects such as energy loss and straggling. These effects give rise to an asymmetric shape of the spectra, which is discussed in more detail by Wojciechowski *et al.*[7] and by

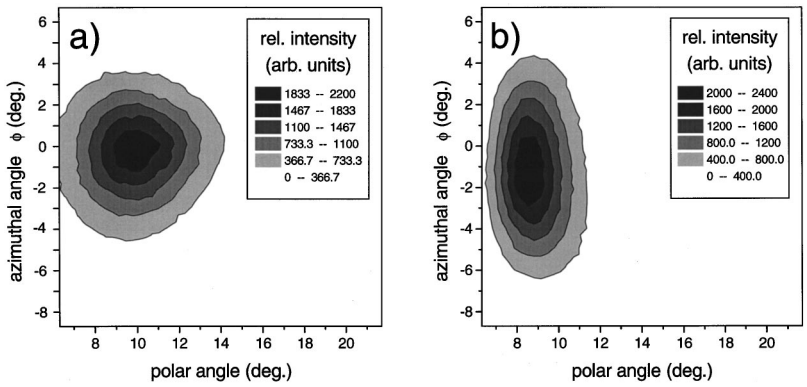

FIG. 2. Spatial distributions of a forward scattered grazing 2.5 keV Ne^+-beam, as seen by the PSD detector. The left plot (a) shows the profile due to high-indexed primary beam incidence and the right one (b) results from low-index scattering.

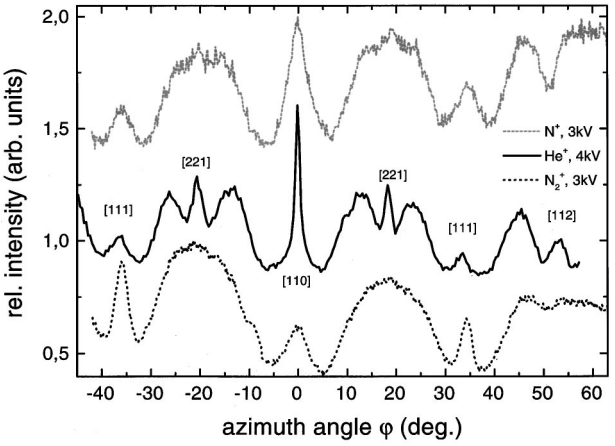

FIG. 3. Azimuth spectra of a typical 1×1-fcc(110)-surface [here Pd(110)] with He^+, N^+, and N_2^+ at different energies in surface channeling geometry measured with the small aperture TOF detector ($\Psi=5°$, $\Theta=10°$, $\phi=0°$).

Närmann *et al.*[23–25] These authors use analytic functions to describe the energetic distributions of the forward scattered beam; we found the best agreement with our experimental results when fitting a universal so-called exponentially modified Gauss function (EMG):

$$I=\frac{a_0}{2a_3}\exp\left(\frac{a_2^2}{2a_3^2}+\frac{E-a_1}{a_3}\right)\left\{1+\mathrm{erf}\left[\frac{\sqrt{2}}{2}\left(\frac{a_1-E}{a_2}-\frac{a_2}{a_3}\right)\right]\right\}. \tag{3.2}$$

E is the kinetic energy within the laboratory system, $I(E)$ the intensity. The parameter a_0 describes the area, a_1 the center, a_2 the width, and a_3 the distortion of the distribution function, respectively. A function of the type Eq. (3.2) has been *ab initio* derived by Remizovich *et al.*[26] from the Boltzmann statistics for the small angle approach, taking into account the inelastic energy losses for different trajectories leading to a given scattering angle. In the work of Närmann *et al.*, the reason for the asymmetry is different, namely the energy loss straggling due to electron exchange processes between the surface and the projectile while moving along its trajectory.

For molecule scattering under channeling conditions, we observe a surprising behavior: For primary energies not being too low, the ''hat'' in the spectra, which is usually attributed to the surviving molecules, cannot be fitted by one single EMG function anymore [Fig. 4(b)]. At least two EMG functions are superimposed here, hence the complete spectrum consists of three peaks. In the next section it will be shown that the sharp additional peak is not—as intuitively expected—due to surviving molecules but rather the result of a certain class of fragmentation products. The effect mainly occurs under surface-channeling conditions where a large amount of molecules scatters between surface atomic rows before being dissociated due to the forces active during collisions with target atoms. Since this effect is mainly observed when scattering along low-indexed directions, it is of interest to investigate the scattering from the more corrugated Pt(110)(1×2) surface. In Fig. 5, the results are shown for the specularly reflected particles as well as for detection at an increased azimuthal angle ϕ in the wing of the PSD profile [Fig. 2(b)—the angle ϕ is obtained when rotating the TOF

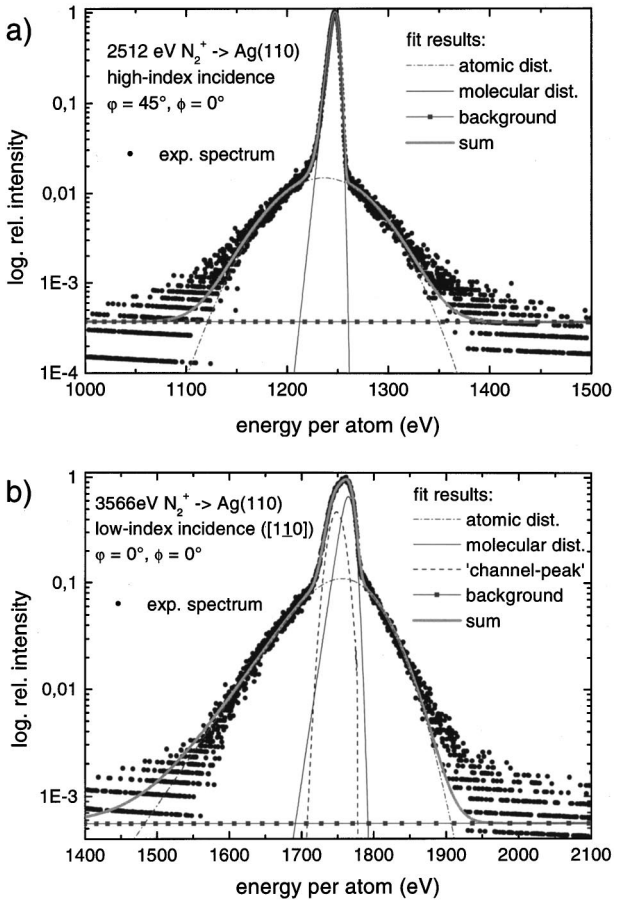

FIG. 4. Typical energy spectra, converted from time-of-flight measurements. The intensity scale is plotted logarithmically. (a) In most cases, the total spectrum is a superposition of one atomic and one molecular distribution, its contributions are determined by fitting EMG functions. (b) In case of low-index scattering (for high enough primary energies), an additional distribution due to the axial surface channeling appears. The energetic width of this ''channel peak'' is comparable to the molecular one.

detector for fixed φ, Ψ, and Θ]. These spectra, showing surprisingly different shapes, are further analyzed in Figs. 5(b) and 5(c), respectively. Obviously, the additional distribution is only present for specular reflection [Fig. 5(b)], indicating that the respective atoms are axially guided by the surface semichannels. The atoms are subsequently focused into a very small range around the specular direction. Away from the specular reflection, the sharp distribution is due to scattered molecules only [Fig. 5(c)].

The peaks obtained from the outlined fitting procedure can be used to calculate the fraction of surviving molecules via integration of the corresponding distributions:

$$Y=\frac{\frac{1}{P_{\mathrm{N}_2}}\mathcal{N}(\mathrm{N}_2)}{\frac{1}{P_{\mathrm{N}_2}}\mathcal{N}(N_2)+\frac{1}{2P_{\mathrm{N}}}\mathcal{N}(\mathrm{N})}, \tag{3.3}$$

where $\mathcal{N}(X)$ is the total detected area and P_X the velocity-dependent detection probability of particles of species X.[27]

Figure 6 displays the experimentally obtained molecular yields $Y(\mathrm{N}_2)$ as a function of the projectile energy E_0. It is obvious, that $Y(\mathrm{N}_2)$ depends on the target (Ag, Pt, or Pd) as

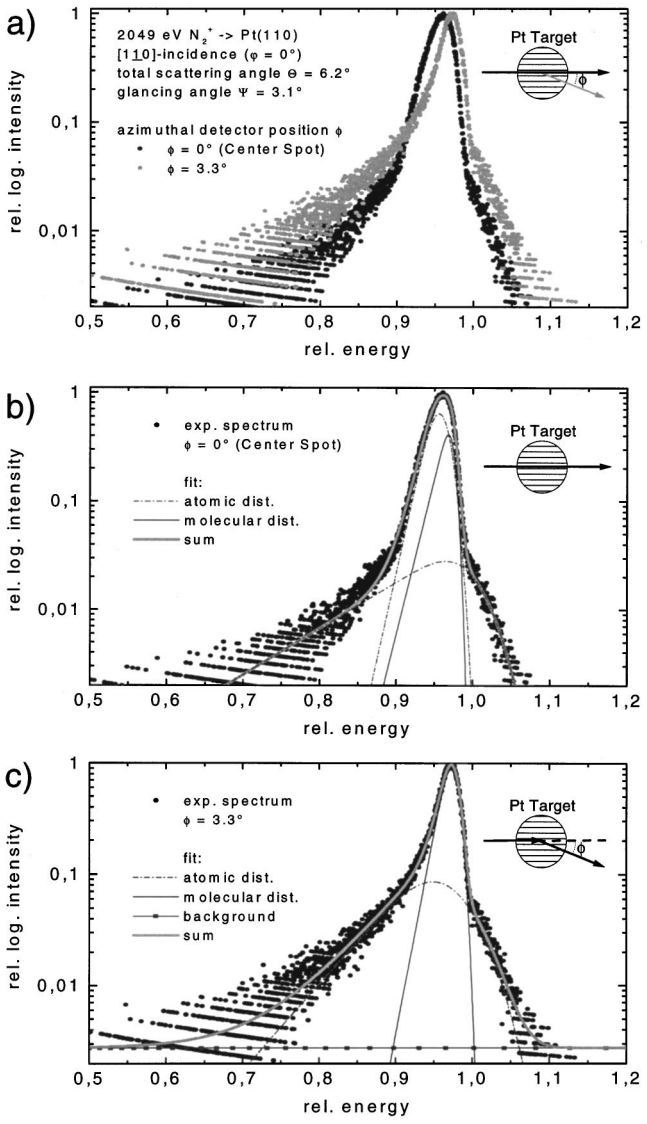

FIG. 5. Energy spectra of N_2^+ scattered off the 1×2-reconstructed Pt(110) for grazing incidence along the $[1\bar{1}0]$-semichannels ($\varphi=0°$). The two spectra are measured at different azimuthal detector positions: The center spot ($\phi=0°$) and a position slightly outside the specularly reflected beam ($\phi=3.3°$) (a). The underlying geometries are shown in the insets. Obviously, the ''channeled'' nitrogen fragments are focused into a small region centered in the plane of scattering. Here, the atomic distribution prevails in the narrow ''hat'' of the spectrum (b), but gives way to the molecular contribution when turning the detector off center (c).

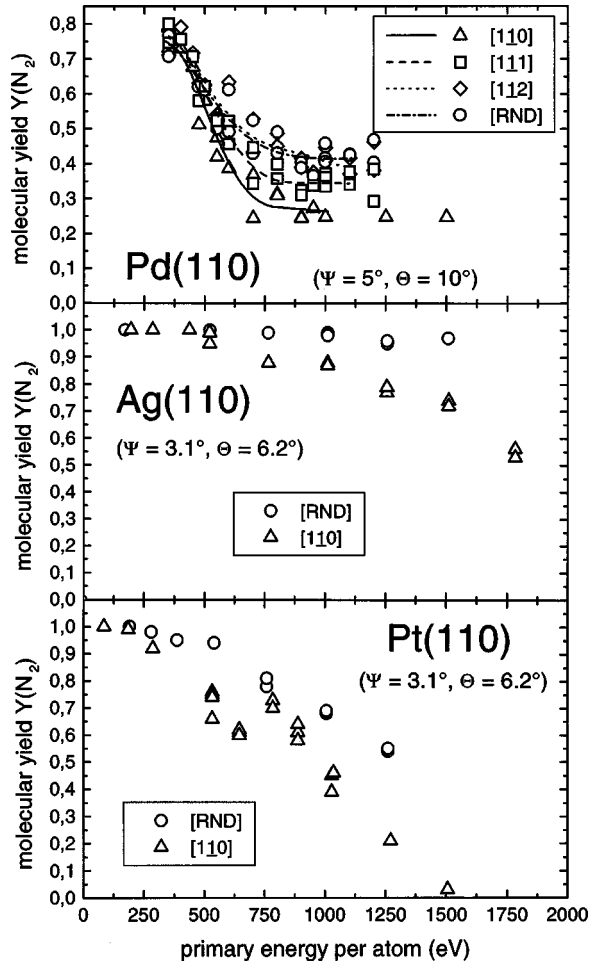

FIG. 6. Molecular yields obtained from scattering experiments on palladium, silver, and platinum, each for both the random- and the $[1\bar{1}0]$-direction under grazing incidence [$\Psi=5°$ and $\Theta=10°$ for Pd(110), $\Psi=3.1°$ and $\Theta=6.2°$ for Ag(110) and Pt(110), $\phi=0°$ in all cases]. In the top plot, lines help to guide the eye; the relatively high dissociation rates are due to the steeper incidence, whereas the difference between Pt(110) and Ag(110), especially for the random direction, might result from the more corrugated 1×2-reconstruction on platinum.

well as on the azimuthal angle of incidence φ. It has to be noted here, that the Pd results (top graph) have been calculated based on a simple Gaussian fitting procedure, which turned out to be less accurate and reliable than our new method using formula 3.2. However, the same trend is visible for all cases: Starting with comparable molecular yields for all orientations in the low-energy region, a clear azimuth-dependent behavior becomes apparent for higher energies. Obviously, the molecular yield for the $[1\bar{1}0]$-scattered particles decreases faster with increasing energies than for higher indexed directions, though for the 1×2-reconstructed Pt(110)-surface, the difference between scattering along random and $[1\bar{1}0]$-direction is not as clear as for the two 1×1-surfaces. No remarkable difference can be seen between

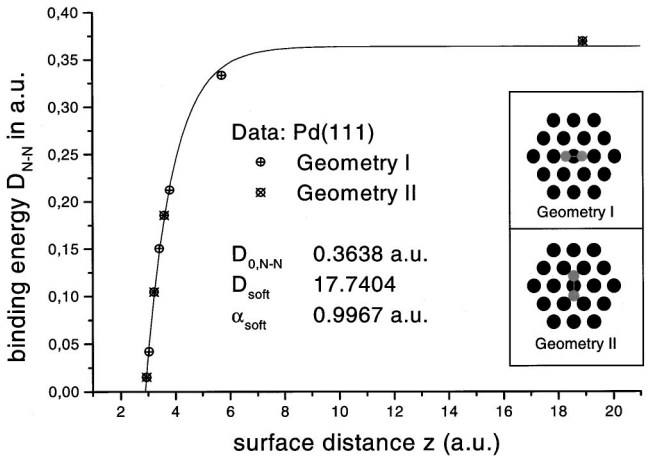

FIG. 7. Calculated N–N binding energies as a function of the molecule-surface distance on Pd(111). The molecule is placed upon a top site, ''lying'' parallel to the surface with its axis oriented along $[1\bar{1}0]$ (geometry I) and [001](geometry II), respectively. The curve is a fit using Eq. (4.11).

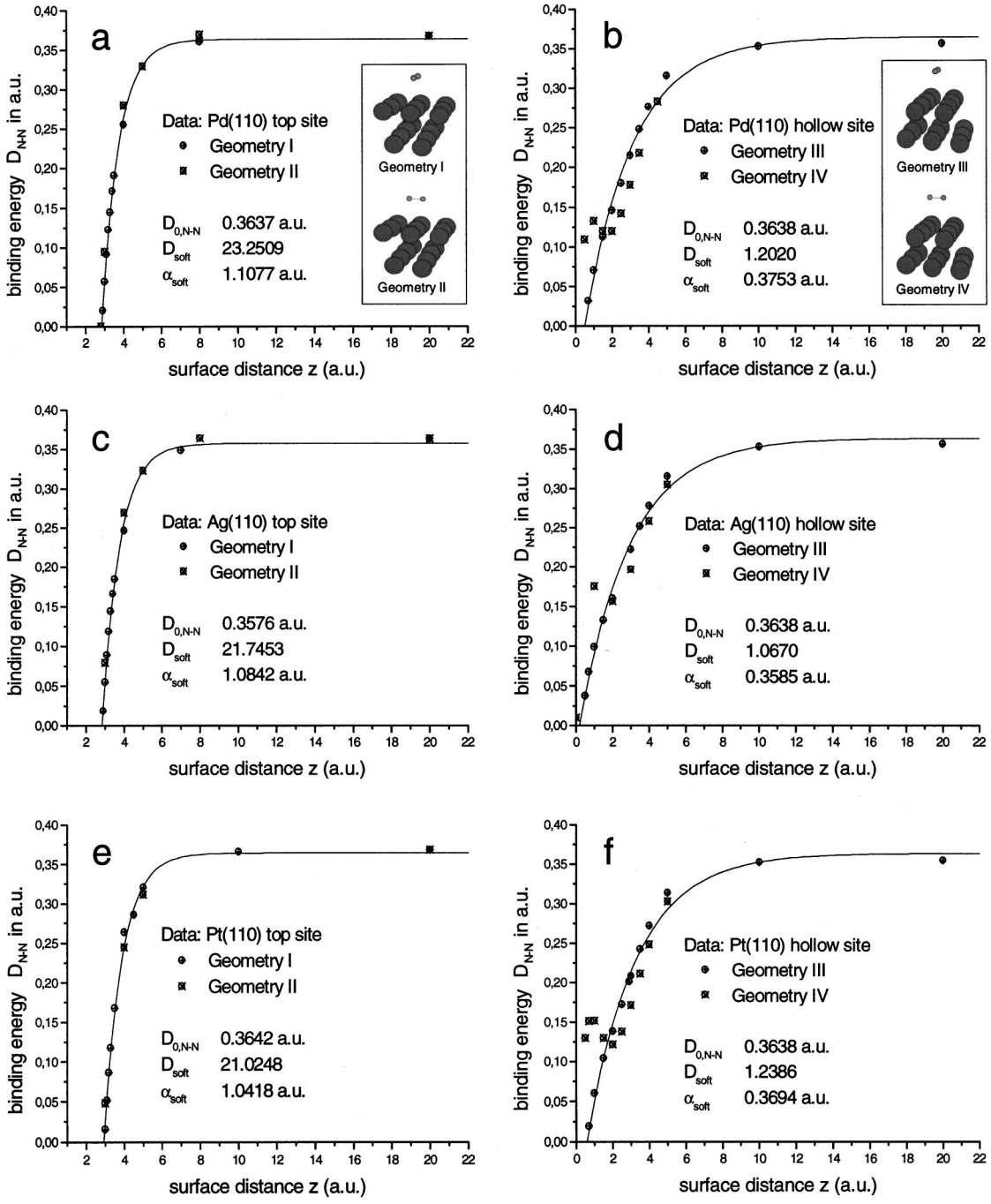

FIG. 8. Calculated N–N binding energies of a nitrogen molecule adsorbed on Pd, Ag, and Pt(110)-surfaces. Adsorption sites are ''on top''[(a), (c), and (e)] and ''hollow'' positions [(b), (d), and (f)]. The molecular axis lies parallel to the $[1\bar{1}0]$-direction (geometry I and III) or to the [001] -direction (geometry II and IV) as illustrated in the insets. The curve is a fit using Eq. (4.11).

$[1\bar{1}2]$-and random direction in the case of Pd; but their survival probabilities exceed those of $[1\bar{1}0]$ and $[1\bar{1}1]$ all over the studied energy range.

IV. SIMULATION

A. Motivation

In a recent paper we predicted on the base of CT calculations, that the dissociation of N_2 scattered off Pd(111) depends on the azimuthal angle of incidence.[5] Qualitatively, these results are in agreement with the experimental results presented in the last chapter, although a good quantitative agreement is not observed (see Fig. 9). Especially for the low-indexed directions of the (110)-surfaces under study, the code is not able to reproduce the molecular yield as a function of E_0. Obviously, an important part of the molecule–surface interaction is neglected in the purely classical description of the scattering process as done so far.[5] In the following, we will show, that the model can be significantly improved by introducing a weakening of the intramolecular bond as a function of the electron density of the surface as sampled by the N_2.

TABLE I. Parameters of the N_2–Pd(111) PES (Ref. 5) (atomic units).

R_0	$D_{0,\mathrm{N-Pd}}$	$\alpha_{\mathrm{N-Pd}}$	$r_{0,\mathrm{N-Pd}}$	$D'_{0,\mathrm{N-Pd}}$	$\alpha'_{\mathrm{N-Pd}}$	$r'_{0,\mathrm{N-Pd}}$	χ	$D'_{0,\mathrm{N-N}}$	$\alpha'_{\mathrm{N-N}}$	$r'_{0,\mathrm{N-N}}$
1.25	0.061	1.05	3.535	0.018	1.3	3.8	0.05	0.4225	1.398	2.059

B. Current model

The model used so far in the SCADIM code is fully described in our recent publication,[5] therefore only a short outline is presented here. The simulation is based on a classical calculation of the molecule–surface interaction via realistic six-dimensional potential energy surfaces (PES). This analytical PES, based on *ab initio* density functional theory (DFT) cluster calculations and empirical data, has the form

$$\mathbf{V}=\begin{pmatrix} V_1 & V_{12} \\ V_{21} & V_2 \end{pmatrix}. \tag{4.1}$$

V_1 embodies the diabatic N–Me PES, V_2 the diabatic N_2–Me PES. The coupling terms must obey $V_{12}=V_{21}$ since the Hamiltonian is Hermitian. Diagonalization of $\mathbf{V}$ yields the adiabatic PES describing the ground state and an excited state of the N_2–Pd system, where only the former is of interest for us:

$$V(\mathbf{r}_1,\mathbf{r}_2)=\tfrac{1}{2}\{[V_1(\mathbf{r}_1,\mathbf{r}_2)+V_2(\mathbf{r}_1,\mathbf{r}_2)] - \sqrt{[V_1(\mathbf{r}_1,\mathbf{r}_2)-V_2(\mathbf{r}_1,\mathbf{r}_2)]^2+4V_{12}(\mathbf{r}_1,\mathbf{r}_2)^2}\}. \tag{4.2}$$

The $\mathbf{r}_i$ are the positions of the N_2 constituents. The diabatic interaction potential of the two N atoms with the surface atoms is assumed to be the sum of a repulsive N–N potential and binding N–Me potentials:

$$V_1(\mathbf{r}_1,\mathbf{r}_2)=V^{\mathrm{ZBL}}_{\mathrm{N-N}}(r)+\sum_{i=1}^{2}\sum_{j=1}^{n} V_{\mathrm{N-Me}}(R_{ij}), \tag{4.3}$$

where r is the N–N distance, R_{ij} is the distance between the ith N atom and jth metal atom and n is the number of surface atoms interacting with the molecule. Since the N–N interaction is repulsive in this state, $V^{\mathrm{ZBL}}_{\mathrm{N-N}}$ is taken here as a screened Coulomb potential. Morse type potentials usually provide a good representation of the attractive part of the N–Me dimer interaction. For the pair potentials $V_{\mathrm{N-Me}}(R_{ij})$, we found out that they are not sufficient to describe the small impact parameter interactions reached at higher beam energies. Here again, the ZBL potential describes the repulsive interaction for short distances $R_{ij}\to 0$ more exactly. In order to get a smooth transition (at a distance R_0) between the high energy region via $V^{\mathrm{ZBL}}_{\mathrm{N-Me}}$ and the low energy part with the Morse potential

$$V^{\mathrm{Morse}}_{\mathrm{N-Me}}(R_{ij})=D_{0,\mathrm{N-Me}}(1-e^{-\alpha_{\mathrm{N-Me}}(R_{ij}-r_{0,\mathrm{N-Me}})})^2, \tag{4.4}$$

we choose

$$V_{\mathrm{N-Me}}(R_{ij})=\frac{1-\tanh(R_{ij}-R_0)}{2}V^{\mathrm{ZBL}}_{\mathrm{N-Me}}(R_{ij}) + \frac{1+\tanh(R_{ij}-R_0)}{2}V^{\mathrm{Morse}}_{\mathrm{N-Me}}(R_{ij}). \tag{4.5}$$

In the same way, the diabatic N_2–Me potential is defined as

$$V_2(\mathbf{r}_1,\mathbf{r}_2)=V'^{\mathrm{Morse}}_{\mathrm{N-N}}(r)+\sum_{i=1}^{2}\sum_{j=1}^{n} V'_{\mathrm{N-Me}}(R_{ij}), \tag{4.6}$$

with

$$V'_{\mathrm{N-Me}}(R_{ij})=\frac{1-\tanh(R_{ij}-R_0)}{2}V^{\mathrm{ZBL}}_{\mathrm{N-Me}}(R_{ij}) + \frac{1+\tanh(R_{ij}-R_0)}{2}V'^{\mathrm{Morse}}_{\mathrm{N-Me}}(R_{ij}) \tag{4.7}$$

and

$$V'^{\mathrm{Morse}}_{\mathrm{N-Me}}(R_{ij})=D'_{0,\mathrm{N-Me}}(1-e^{-\alpha'_{\mathrm{N-Me}}(R_{ij}-r'_{0,\mathrm{N-Me}})})^2. \tag{4.8}$$

The N–N interaction is now attractive and can be described by a Morse potential:

$$V'^{\mathrm{Morse}}_{\mathrm{N-N}}(r)=D'_{0,\mathrm{N-N}}(1-e^{-\alpha'_{\mathrm{N-N}}(r-r'_{0,\mathrm{N-N}})})^2. \tag{4.9}$$

Depending on which V_{12} is chosen for the final PES, the parameters $D'_{0,\mathrm{N-N}}$, $\alpha'_{\mathrm{N-N}}$ and $r'_{0,\mathrm{N-N}}$ have to be modified from the exact values for the N–N Morse potential[28] in such a way that Eq. (4.2) results in the correct N–N interaction potential of gas phase N_2 for an infinite molecule-surface distance again. This modification becomes necessary due to the hybridization of $V'^{\mathrm{Morse}}_{\mathrm{N-N}}$ and $V^{\mathrm{ZBL}}_{\mathrm{N-N}}$.

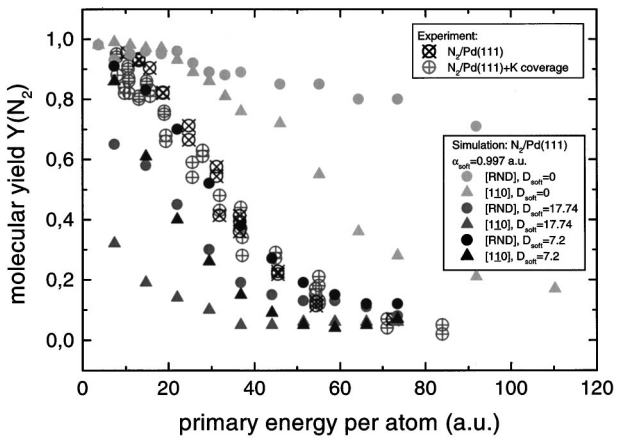

FIG. 9. Molecular yields from N_2 scattering off Pd(111) [experimental data from our recent publication (Ref. 5)] under grazing incidence ($\Psi=5°$, $\Theta=10°$, $\phi=0°$). Simulations (full symbols) are made using the ''new'' model with different softening-parameters D_{soft}; circles are used for high-indexed directions, triangles indicate scattering along $[1\bar{1}0]$. The case $D_{\mathrm{soft}}=0$ (light gray symbols) has already been discussed (Ref. 5). $D_{\mathrm{soft}}=17.74$ is the static softening (gray symbols) obtained from *ab initio* DFT calculations for a top adsorption site (Sec. IV D). We find best agreement with the effective parameter $D_{\mathrm{soft}}=7.2$ (random direction).

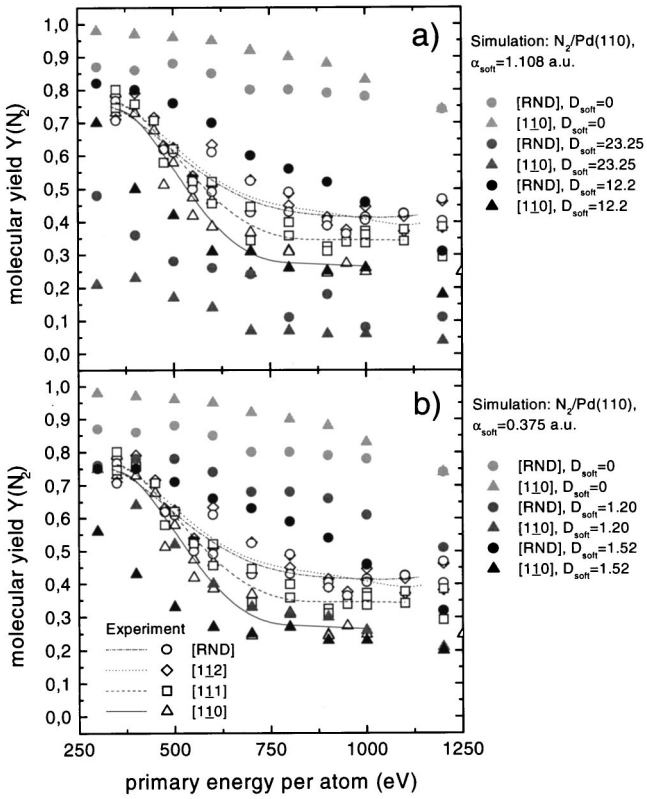

FIG. 10. Molecular yields from N_2 scattering off Pd(110) (Fig. 6) for high-indexed directions (circles) and scattering along $[1\bar{1}0]$ (triangles). The simulations (full symbols) are made with different softening parameters: $D_{\text{soft}}=0$ (light gray) reflects the ''old'' model calculations. When switching to the ''new'' model ($D_{\text{soft}}>0$), the agreement improves qualitatively and quantitatively. In (a), we used the softening parameters from Fig. 8(a), in (b) from Fig. 8(b).

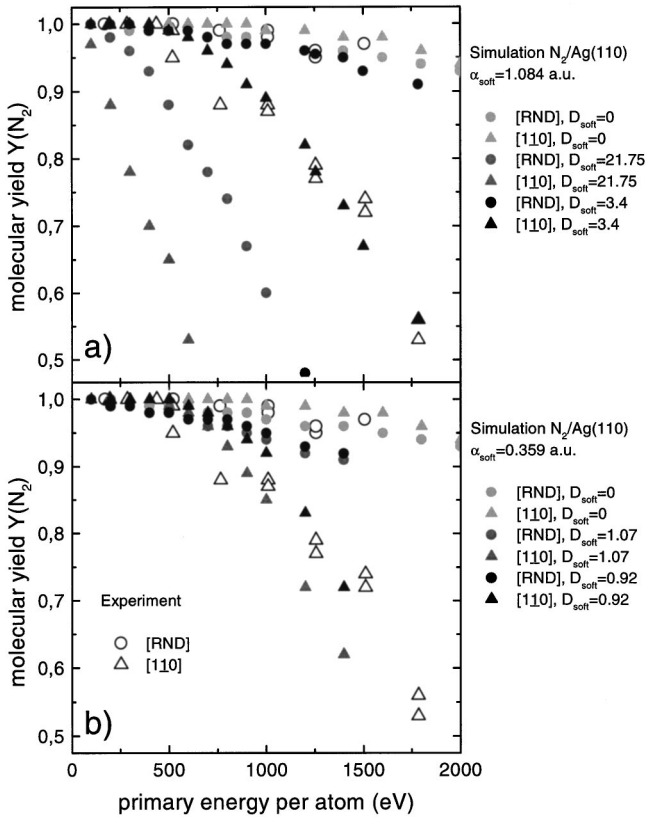

FIG. 11. Molecular yields from scattering N_2 off Ag(110) (Fig. 6). The symbols are explained under Fig. 9. In (a), we used the initial softening parameters from Fig. 8(c) (top site), in (b) from Fig. 8(d) (hollow site).

The coupling term V_{12} mainly influences the dissociation barrier and stays as a free mixing parameter in our calculation:

$$V_{12}=\chi. \tag{4.10}$$

Within a reasonable range, the choice of this parameter and therefore the form of the dissociation barrier however turned out to be minor importance for the result. This can be expected for the system under study where the translational energies are in the keV range.

The parameters used in Eqs. (4.4) and (4.8) as well as R_0 are obtained by fitting V_1 and V_2 to results from corresponding DFT cluster calculations using the commercial DFT software DMOL[29] and experimental data.

C. Improving the model

As stated early in this article, we improve the simulation by explicitly including a static softening of the intramolecular bond as a function of the local electron density. This softening, caused by the screening of metal conduction band electrons, plays an important role in the dissociation process of the systems under study. Henriksen *et al.*[12] use in their work on the dissociative chemisorption of N_2 on rhenium use a similar approach but with a coordinate-dependent parameter $D'_{\text{N-N}}(R_{ij})$ replacing $D'_{0,\text{N-N}}$ in Eq. (4.9). The two other parameters in Eq. (4.9) are expected to be only weakly dependent on R_{ij} and therefore kept constant. Since we work with projectiles of much higher translational energy, the lateral change of the surface electron density when moving mainly parallel to the surface is expected to average out. Therefore, we treat $D'_{\text{N-N}}$ as a function of the molecule-surface-distance only:

$$D'_{\text{N-N}}(z)=D'_{0,\text{N-N}}(1-D_{\text{soft}}e^{-\alpha_{\text{soft}}z}) \tag{4.11}$$

and therefore, Eq. (4.9) changes to

$$V'^{\text{Morse}}_{\text{N-N}}(r,z)=D'_{\text{N-N}}(z)(1-e^{-\alpha'_{\text{N-N}}(r-r'_{0,\text{N-N}})})^2. \tag{4.12}$$

$D'_{0,\text{N-N}}$ is still the binding energy of the gas-phase N_2 for an infinite molecule-surface distance according to the conditions described in Sec. IV B. D_{soft} and α_{soft} are new parameters which we take from DFT calculations as described in

TABLE II. Parameters of the N_2–Ag(110) PES (atomic units).

R_0	$D_{0,\text{N-Ag}}$	$\alpha_{\text{N-Ag}}$	$r_{0,\text{N-Ag}}$	$D'_{0,\text{N-Ag}}$	$\alpha'_{\text{N-Ag}}$	$r'_{0,\text{N-Ag}}$	χ	$D'_{0,\text{N-N}}$	$\alpha'_{\text{N-N}}$	$r'_{0,\text{N-N}}$
2.362	0.057	0.774	3.32	0.0016	0.83	4.6	0.05	0.4225	1.398	2.059

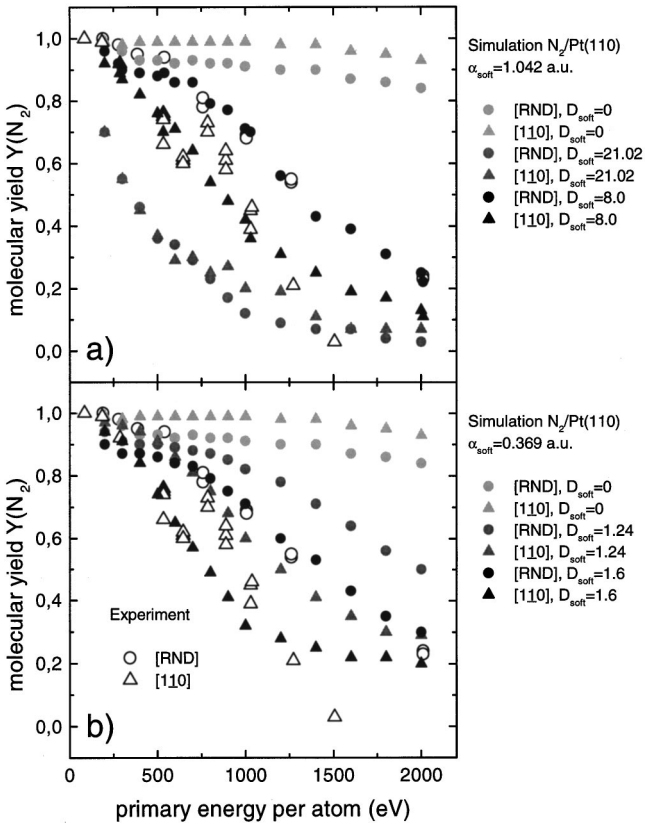

FIG. 12. Molecular yields from scattering N_2 off Pt(110)(1×2) (Fig. 6). The symbols are chosen as explained under Fig. 9. In (a), we used the initial softening parameters from Fig. 8(e) (top site), in (b) from Fig. 8(f) (hollow site).

the following section. With this small upgrade, an effective softening of the intramolecular bond is recomputed in each integration step along the trajectory of the molecule. Neither any lateral structure information nor time-dependent relaxation effects are taken into account.

D. Determination of the softening effect

To get a first impression of the effect of a z-dependent intramolecular bond, we use the system N_2/Pd(111) and make a comparison to the respective CT results in Ref. 5. The PES is already known from this work, hence we only have to find the softening parameters for Eq. (4.11). Since to our knowledge no experimental or theoretical data are available for this system, we perform *ab initio* DFT cluster calculations to estimate the N–N binding energies $D_{\mathrm{N-N}}$ at different molecule-surface distances z, i.e., the static case.

We use a procedure similar to the one for computing the N–Me and N_2–Me interaction potentials[5] for Eqs. (4.4) and (4.8). The surface is approximated by a substrate cluster of about 20–50 atoms arranged in the corresponding geometry of the surface under investigation. No relaxation effects are taken into account; the position of the metal atoms is strictly given by the bulk fcc structure and the (111)- and (110)-surface, respectively. The nitrogen molecule is now placed with its axis lying parallel to the cluster surface at a given distance z. Two adsorption sites are probed for the (110)-surfaces, the top site and the hollow site; only the top site is used for Pd(111) since this is a closely packed surface and the differences between the adsorption sites are expected not to vary much. The values obtained for the top sites are upper limits for the effective screening effect, since the local electron density is highest for a given z at that position.

For each adsorption site, two molecule orientations are examined: the molecule is either oriented with its axis parallel to the $[1\bar{1}0]$-direction or perpendicular to that. So, for each given adsorption site, molecule orientation, and surface distance z, we calculate the total energy of the system for different intermolecular N–N distances r using the commercial DFT software DMol.[29] The results of each study can then be fitted by Morse type potentials as described by Eq. (4.12). Figure 7 shows the results for the Pd(111) surface. Equation (4.11) is used in this plot for fitting the $D_{\mathrm{N-N}}(z)$. It is seen clearly, that the softening of the molecular bond is not sensitive to the lateral orientation of the molecule (for this adsorption site). Indeed, also the results for N_2 on top sites of the Pd(110) [Fig. 8(a)], Ag(110) [Fig. 8(c)], and Pt(110) surfaces [Fig. 8(e)] show no remarkable difference between the two orientations with respect to the $[1\bar{1}0]$-chain. However, when the molecule is placed upon a hollow site, a slight divergence of the $D_{\mathrm{N-N}}(z)$ becomes apparent for small z values due to the distortion of the surface top row atoms [Figs. 8(b), 8(d), and 8(f)]. As a consequence, our model which neglects any lateral dependency is expected to have a weakness in describing the interaction in particular for scattering along the $[1\bar{1}0]$ surface channels at high (perpendicular) energies, where the particles reach small impact parameters.

For the Pt(110)-calculations [Figs. 8(e) and 8(f)], a 1×1 surface structure instead of the real 1×2 is used considering the small size of the cluster.

E. Results

1. N_2/Pd(111)

This system has been studied in detail previously[5] and is reexamined here, to have a direct comparison of results obtained with and without the softening of the bonds. Table I summarizes the parameters used for the simulation. Figure 9 shows the experimental molecular yields of N_2 scattered off Pd(111) as a function of the energy, compared with CT results obtained with three different softening parameters. A high-indexed crystallographic direction is chosen, which for the (111)-structure is well encountered at $\varphi=35°$. The first set of calculations (light gray symbols) is also taken from

TABLE III. Parameters of the N_2–Pt(110) PES (atomic units).

R_0	$D_{0,\mathrm{N-Pt}}$	$\alpha_{\mathrm{N-Pt}}$	$r_{0,\mathrm{N-Pt}}$	$D'_{0,\mathrm{N-Pt}}$	$\alpha'_{\mathrm{N-Pt}}$	$r'_{0,\mathrm{N-Pt}}$	χ	$D'_{0,\mathrm{N-N}}$	$\alpha'_{\mathrm{N-N}}$	$r'_{0,\mathrm{N-N}}$
1.662	0.0516	0.86	3.37	0.0095	1.10	4.17	0.05	0.4225	1.398	2.059

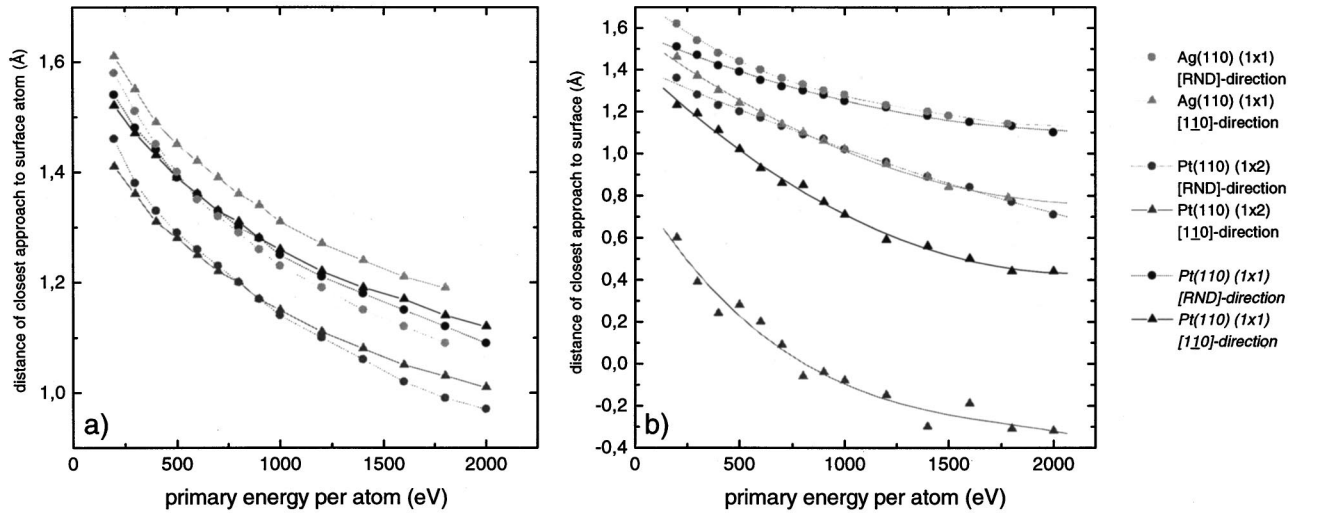

FIG. 13. Average distances of closest approach from the N_2-molecule constituents to the nearest surface atoms (a) and the plane of first layer atoms (b), respectively, obtained from simulations for the Ag(110)(1×1), Pt(110)(1×2), and a ''virtual'' Pt(110)(1×1) surface.

Ref. 5, corresponding to $D_{\text{soft}}=0$ in our model. Obviously, the simulated dissociation efficiency of the N_2 molecules is much too low. The CT results based on the softening parameters $D_{\text{soft}}=17.74$ and $\alpha_{\text{soft}}=0.997$ a.u. as obtained in the previous section are displayed as gray symbols in the same figure. As expected, the dissociation efficiency is too high when adopting these maximum values. We find good agreement with the experimental results by lowering D_{soft} to an effective value of 7.2 and keeping $\alpha_{\text{soft}}=0.997$ a.u. (black symbols). This effective softening parameter $D_{\text{soft}}=7.2$, obtained by fitting, describes the average screening allocated to the molecule.

2. N_2/Pd(110)

The first (110)-surface investigated with the modified code was chosen to be Pd(110). Since it is based on the same lattice as the Pd(111) surface, for reason of simplicity the parameters from Table I are used here again. The calculated results are shown in Fig. 10. As for all (110)-faces, the high-indexed direction [labeled with (RND)] is found at $\varphi=45°$. Similar to the Pd(111) surface, the dissociation efficiency is too low using $D_{\text{soft}}=0$, and using the static softening parameters from Figs. 8(a) and 8(b), the screening is slightly over- and underestimated, respectively. We could achieve the best agreement when either lowering the effective D_{soft} from 23.25 [Fig. 8(a)] to 12.2 with $\alpha_{\text{soft}}=1.108$ a.u. [Fig. 10(a)] or when raising it from 1.20 [Fig. 8(b)] to 1.52 with $\alpha_{\text{soft}}=0.375$ a.u. [Fig. 10(b)].

3. N_2/Ag(110)

The interaction of N_2 with the Ag and Pt surfaces was studied under more grazing incidence than in the respective study on Pd surfaces. Instead of $\Psi=5°$ and $\Theta=10°$ we now use $\Psi=3.1°$ and $\Theta=6.2°$, respectively, in order to reduce the perpendicular component of the kinetic energy. Figure 11 shows the comparison between experiment and simulation for Ag(110). The parameters we determine for the N_2/Ag(110)-PES are given in Table II. Again, the fragmentation calculated with $D_{\text{soft}}=0$ is too low. Using the static softening parameters from Figs. 8(c) and 8(d), the dissociation becomes too strong. A good compromise is found with $D_{\text{soft}}=3.4$ for calculations using $\alpha_{\text{soft}}=1.084$ a.u. from top-site adsorption [Fig. 8(c)]. Using $D_{\text{soft}}=0.92$ for the hollow-site softening parameter with $\alpha_{\text{soft}}=0.359$ a.u. from Fig. 8(d), the agreement is worse. This cannot be improved using the hollow-site α_{soft} and further adjustment of D_{soft}.

4. N_2/Pt(110)

Pt(110) plays an important role in our work, since the properly prepared surface is 1×2-reconstructed in the missing-row structure, in contrast to the other surfaces under study which are unreconstructed at room temperature. In our experiments, we observe higher molecular fragmentation, and the difference between incidence along high indexed and the $[1\bar{1}0]$-direction is not as pronounced as for the Ag(110)

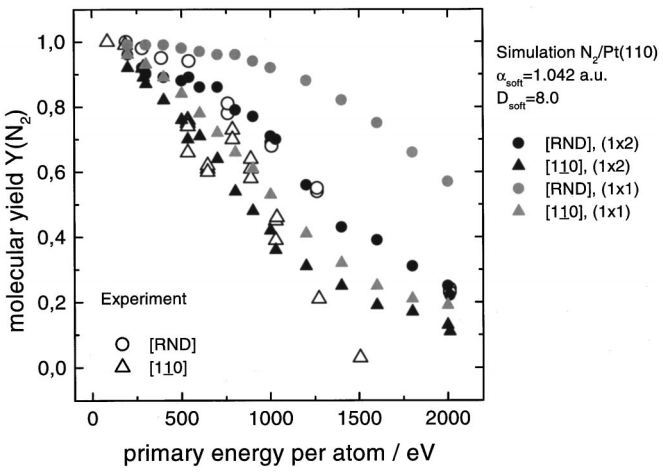

FIG. 14. Molecular yields from scattering N_2 off Pt(110). The simulations are performed using the ''virtual'' Pt(110)(1×1)-surface (light gray symbols) and compared to the real 1×2-structure (black symbols). We used the softening parameters from Fig. 12(a).

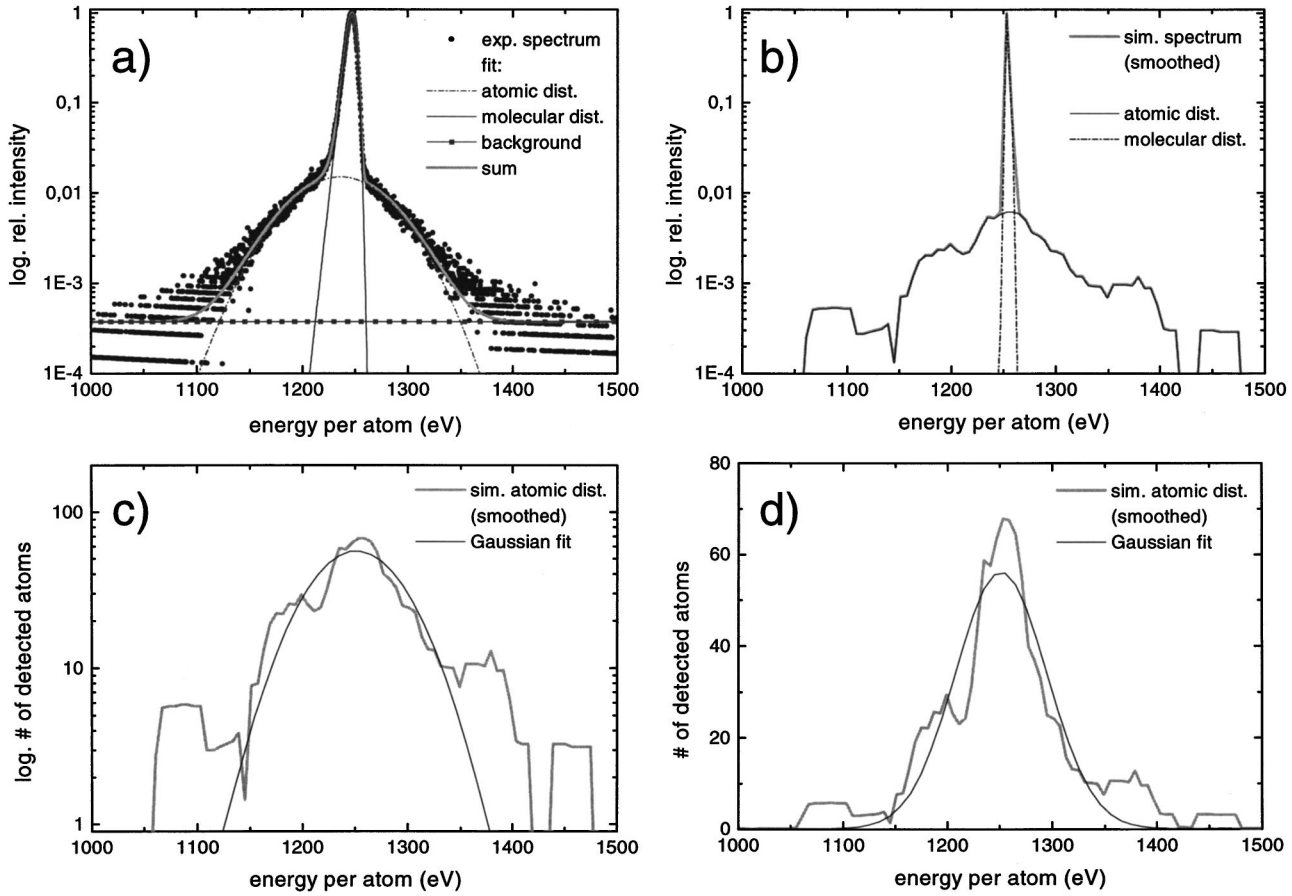

FIG. 15. Experimental (a) and simulated (b) energy spectrum of 2512 eV N_2 scattered off Ag(110) under high-index grazing incidence. The separation of the experimental spectrum is described in Sec. III. The simulated spectrum is automatically separated by the software. The molecular and atomic distributions follow a Gaussian shape, as demonstrated for the latter in logarithmic (c) and linear scale (d).

surface under the same conditions (Sec. III). The simulations reflect this behavior. Figure 12 shows how we achieve the best description when either lowering the effective D_{soft} from 21.02 [Fig. 8(e)] to 8.0 with $\alpha_{\text{soft}}=1.042$ a.u. [Fig. 12(a)] or when raising it from 1.24 [Fig. 8(f)] to 1.6 with $\alpha_{\text{soft}}=0.369$ a.u. [Fig. 12(b)]. Again it turns out, that the former case generally leads to a better agreement than using the softening parameters from the hollow-site geometry as in Fig. 12(b). For this reason, we use the parameters from Fig. 12(a) for our further calculations in the next section. Experimental results obtained under variation of the total scattering angle are interpreted by simulations using the same model with these parameters.[30] The appropriate PES parameters for N_2/Pt(110) are presented in Table III.

V. DISCUSSION

A. General aspects

The fate of a given molecule not only depends on its orientation with respect to the surface normal, but also on the azimuthal orientation of the surface with respect to the beam. For high-indexed directions, the molecule experiences a rather flat surface, unless it is not as strongly corrugated as the Pt(110)(1×2). Negligible contributions of rotational excitation occur during the interaction. For an impact along a low-index direction, however, the molecule constituents scatter rather independently from the walls of the surface semichannels. In these semichannels, the trajectories are longer, consisting of multiple collisions, which usually leads to higher rotational excitation of the molecule compared to the high-index incidence. But this is obviously not the whole truth. As we conclude from our experimental and simulational results, it is important to take the effect of screening into consideration as well. This effect influences the dissociation considerably by lowering the intramolecular binding energy prior to and during the elastic interaction between the projectiles and the surface. Subsequent dissociation, activated by mechanical excitations as rotation and vibration, is therefore promoted. The implementation of the new model is a simple but successful approach to get a qualitative and quantitative interpretation of the experimental data.

B. Pt(110) surface

It has been shown in the previous section, that fragmentation is enhanced for scattering along low-index directions, i.e., a strong dependence on the surface structure exists. In this context, due to its pronounced corrugated structure, the Pt(110)(1×2) surface is a special case. The fragmentation, especially for the high-indexed direction, is strikingly high compared to the 1×1-surface of Ag(110) (see Fig. 6). Within the image of mechanically induced dissociation, it is

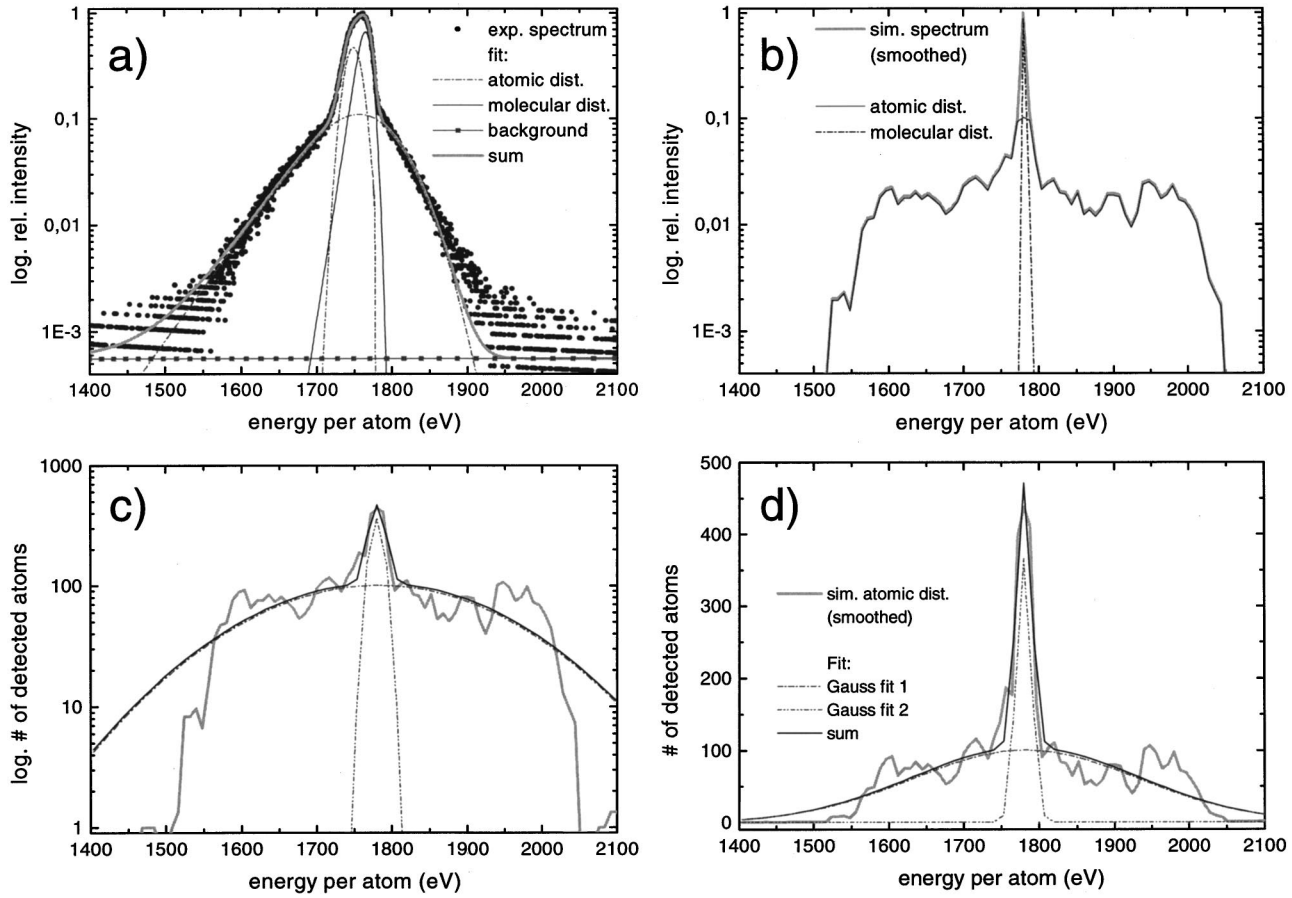

FIG. 16. Experimental (a) and simulated (b) energy spectrum of 3566 eV N_2 scattered off Ag(110) under low-index grazing incidence. The experimental spectrum [same plot as in Fig. 4(b)] shows three components: one molecular and two atomic distributions. Our simulations reflect this behavior: the atomic distribution consists of a ''normal'' broad peak and a surprisingly narrow one (c) and (d). The latter is mainly formed by molecules which dissociate deep inside the channels under strong influence of the softening.

reasonable to suspect the more corrugated missing-row structure being responsible for these higher dissociation rates. Two observables which may shed some light onto this problem are the distance of the closest approach between projectile constituents and surface atoms as well as the penetration depth of the projectiles.[5] A closer look into the distances of the closest approach as a function of the projectile energy (as obtained from our CT calculations) leads to Fig. 13(a).

For the Ag(110) surface, the same behavior as in Ref. 5 is found; the mean distance of the closest approach is larger for scattering along a low-indexed direction, i.e., more but less violent collisions occur in low-indexed directions compared to a high-index geometry. This causes larger fragmentation (Fig. 6) due to enhanced rotational excitation. For the Pt(110)(1×2) surface, the situation changes. Over the whole energy range used in this work, the impact parameters are smaller than the respective values for the unreconstructed surfaces. This gives rise to a larger transfer of projectile translational energy to internal degrees of freedom. In addition, the results for the $[1\bar{1}0]$-direction and the high-indexed direction are almost identical for the Pt(110)(1×2) surface, in contrast to the unreconstructed case. This indicates, that on the Pt surface the fragmentation is not only more effective but also based on a different mechanism as for the 1×1 surfaces. To crosscheck, Fig. 13(a) also displays the average distances of the closest approach for the (fictive) Pt(110)(1×1) surface. These distances are now comparable to the Ag case, even though the results for the two directions are nearly identical, as for the 1×2 case.

Figure 14 shows the impact of the reconstruction on the molecular survival probability: simply switching from 1×2 to 1×1—while preserving all other interaction potentials including the softening parameters increases the molecular survival probabilities remarkably, especially for incidence along the high-indexed direction. Only for scattering along the $[1\bar{1}0]$-direction off Pt(110)(1×2), negative average distances of the closest approach between the molecule and the surface occur in the high energy range [Fig. 13(b)], which means penetration below the plane of the top layer atoms. In general, a closer approach towards the more open 1×2-reconstructed surface is achieved than for the unreconstructed 1×1-faces for both, high- and low-index incidence. Consequently, the effective $D_{\mathrm{soft}}=8.0$, which was determined for the Pt(110)(1×2) surface but also used for the fictive Pt(110)(1×1), is too strong, explaining the fact that the computed dissociation still remains stronger than for Ag(110). The true effective value for Pt(110)(1×1) can be expected to be smaller. Naturally, no experimental data are available for this fictive geometry.

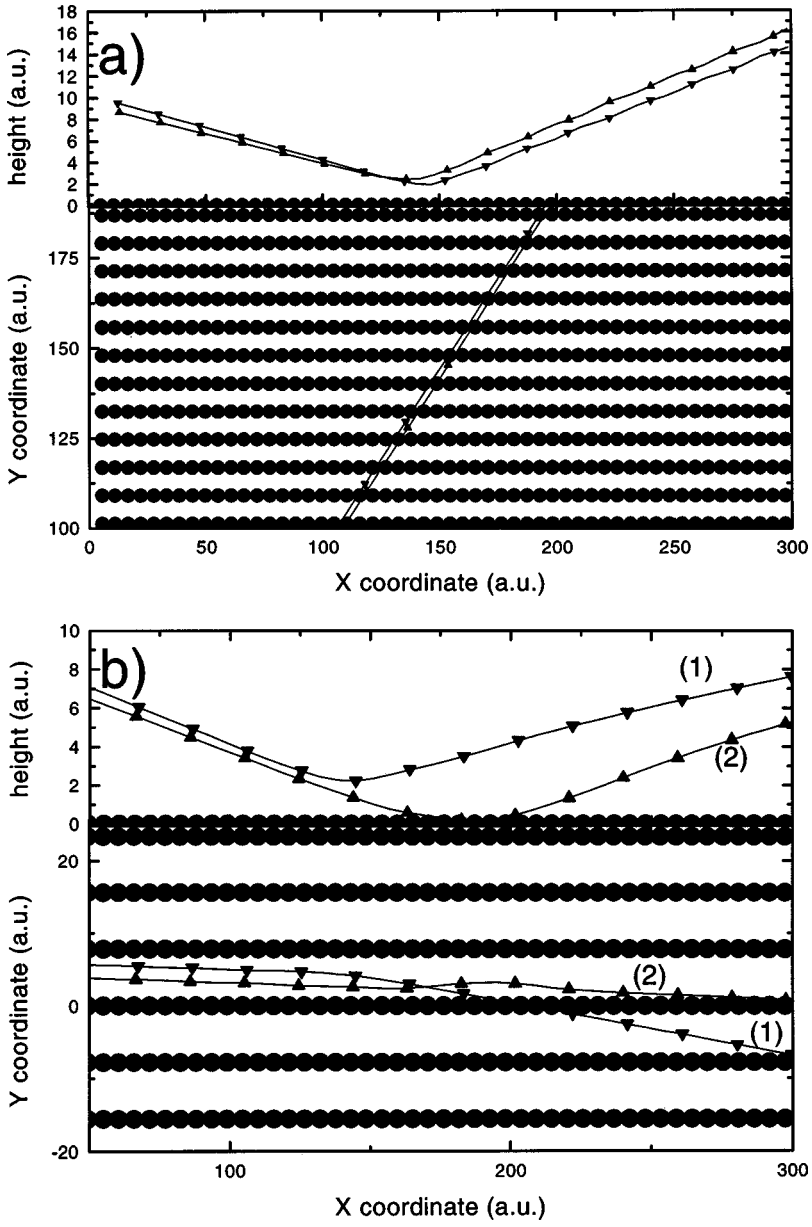

FIG. 17. Trajectories of N_2 molecules (here 2.5 keV) scattered from Ag(110). The situation for high-indexed (random) incident is illustrated in (a), for the low-indexed case in (b). Each plot shows a side and a top perspective. Note the different scaling of the axes.

C. Further consequences of the screening

According to Eq. (3.1), the laboratory energy of the dissociated particles not only depends on E_0, but also on the actual molecular binding energy at the time of its decay as well as on the orientation of the molecule. As a consequence, the fragment distribution has a width of several hundred eV in the energy spectra and can easily be identified that way. Figure 15 compares the measured spectrum of 2512 eV N_2 scattered off Ag(110) in random direction [same spectrum as in Fig. 4(a)] with simulated data. Only one aggravating difference is apparent: The EMG function (Sec. III) provides the best fit for the experimental spectrum, whereas the simulated distributions merely follow an unshifted (with respect to the position of the primary beam) Gaussian shape. This is not surprising, since in our calculations we omitted the inelastic energy losses and straggling effects, which are known to cause the observed energy shift and asymmetry in the measured spectra. The simulated spectra are largely symmetrical. In order to demonstrate their agreement, the separated atomic distribution is extracted from the plot in Fig. 15(b) and compared to its own Gaussian fit in Figs. 15(c) and 15(d) (logarithmic and linear scale), respectively.

An interesting effect occurs for molecular scattering under channeling conditions, unless the primary energies are too low: we observe an additional peak in the hat of the spectra. At least two EMGs are superimposed here, so the complete spectrum consists of three peaks [Figs. 4(b) or 16(a)]. The same question arose in an earlier investigation with the system H_2/Pd(110) at energies around 2 keV.[31] Our first attempt to attribute the additional narrow peak to the molecules resulted in inconsistent survival yields. A closer examination of the simulational results [Figs. 16(b)–16(d)] reveals the problem: Not the molecular but the fragment fraction of the yield gives rise to the second narrow peak in Fig. 16(a). The total fragment fraction in Fig. 16(b), which is further analyzed in Figs. 16(c) and 16(d), consists of two

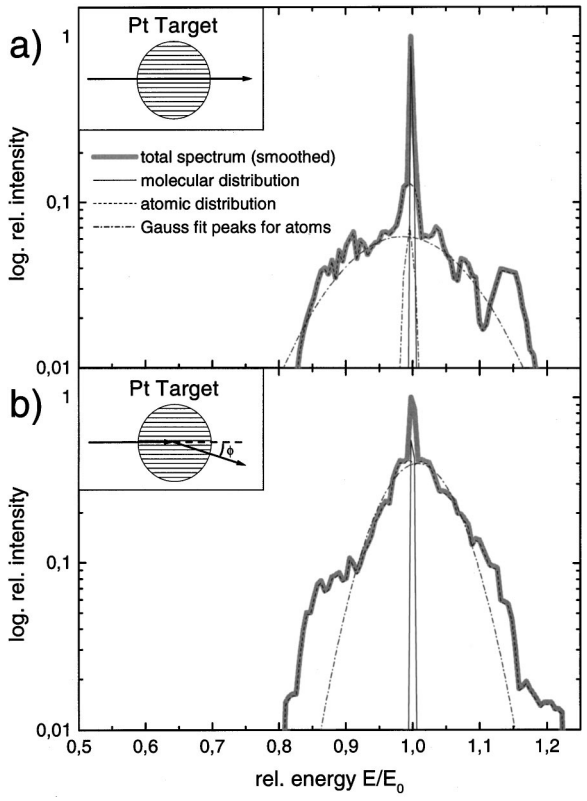

FIG. 18. Simulated energy spectra of 2050 eV N_2 scattered from the 1×2-reconstructed Pt(110) under low-index incidence along the $[1\bar{1}0]$ semichannels ($\varphi=0°$), calculated for two different azimuthal detector positions ϕ. The underlying geometries are indicated in the insets. Analysis of both spectra shows qualitative agreement with the experiment (Fig. 5): In the center spot $\phi=0°$ (a), the fraction of softly dissociated and channeled atoms gives rise to an additional narrow peak which vanishes in the off-centered position $\phi=3.3°$ (b).

superimposed peaks. The broad one is the normal one in analogy of the high-indexed case; the narrow peak is a special feature of the low-index scattering. Here, the geometry of the surface allows a deeper penetration of the N_2 molecules into the semichannels down to the second atom layer. An informative trajectory analysis comparing high- and low-index scattered N_2 projectiles can also be obtained from the simulation. Two representative trajectories of initially bound N atoms for each crystallographic orientation are displayed in Fig. 17.

While for high-indexed incidence [Fig. 17(a)] the trajectories show no remarkable differences in their penetration depths and azimuthal dispersion, mainly two classes of trajectories occur in the low-index case [Fig. 17(b)]:

(i) Particles which impinge on a closely packed top-atom row reach only minimal penetration but scatter with relatively wide azimuthal variation (1). Very short interaction with the surface is the result.

(ii) Constituents which penetrate between the rows and reach respective depths. This channeling also causes significant trajectory lengths. Some of the particles perform ''zig–zag'' trajectories due to multiple scattering from the potential walls of the surface semichannels (2).

It is clearly visible from the statistical evaluation of our simulations, that in case of $[1\bar{1}0]$-incidence, a considerable part of atoms is reflected from up to exactly one interlayer distance deeper. These particles arise from channeling trajectories of type (2) in Fig. 17. Stronger screening in these deeper regions is expected, resulting in a vanishing of the intramolecular binding forces. Consequently, dissociation with zero kinetic energy release according to Eq. (3.1) is observed. The energetic distribution of these ''softly dissociated'' fragments forms the narrow peak as observed experimentally. Compared to the molecular one, this peak is shifted towards lower energies [Fig. 16(a)], since the surviving molecules do not experience such long and deep trajectories and hence less energy loss. This shift is not reproduced by our simulations due to the neglect of inelastic losses.

We showed in Sec. III that not only the energetic, but also the azimuthal distribution of those atoms in the outgoing trajectory which form the sharp energy distribution is limited, since it only appears in the central spot region of the specularly reflected beam. Again, we examine our experimental findings with the help of the simulations. Figure 18 demonstrates the two cases of azimuthal TOF-detector displacement (0° and 3.3° with respect to the direction of the incident beam) referring to Figs. 5(b) and 5(c). We can see from these figures that the principal characteristics of the experimental results are reproduced in the simulations: The sharp energetic peak of the ''softly dissociated'' atoms only appears in the specular geometry [Fig. 18(a)].

VI. SUMMARY AND CONCLUSION

In this work, the interaction of keV N_2^+ molecular ions with metal surfaces under grazing incidence was studied experimentally. The results were compared to classical trajectory calculations. Although it is known that electron transfer processes play a minor role for these systems within a purely classical description no satisfying agreement to experimentally obtained fragmentation yields could be obtained. The dynamic screening of the mutually bound molecular contituents from each other by the presence of the conduction band electrons of the metal play a sizable role for the dissociation process. In our calculations, we can reflect this z-dependent N–N bond weakening by introducing an explicit z dependence of the regular N–N potential. Even a static model independent of the projectile velocity v_{proj} leads to an obvious improvement. Within the model, the parameter D_{soft} reflects the bond dissolution and is determined by comparing experiment and simulation. From the comparison we conclude that screening effects play a crucial role in dissociative scattering of N_2 from metal surfaces, although not in a dynamical way. In the system under study we observe static screening. However, the elastic interaction of the molecule constituents with surface atoms acts as a ''trigger'' for the fragmentation, since we notice a higher amount of rotational excitation and hence more dissociation arising from low-index scattering in comparison to impact along high-indexed directions (first mentioned in Ref. 5).

An interesting result from our study is the identification of a new class of fragments overlapping energetically with the spectrum of scattered intact molecules: under the conditions of axial surface channeling, a large number of mol-

ecules penetrate deep into the semichannels and experience an extreme influence of the screening prior to the elastic interaction. This leads to ''soft dissociation'' with minimal kinetic energy released, as confirmed by the calculations.

ACKNOWLEDGMENTS

This research is supported by the Deutsche Forschungsgemeinschaft (DFG) and the Program of Scientific and Technological Cooperation between Germany and Uzbekistan (Grant No. USB 005-96). T. S. gratefully acknowledges financial support from the Stichting voor Fundamenteel Onderzoek der Materie (FOM) which is supported by the Nederlandse Organisatie voor Wetenschapelijk Onderzoek (NWO).

[1] W. Heiland, in *Low Energy Ion-Surface Interactions*, edited by J. W. Rabalais (Wiley, New York, 1994), p. 313.
[2] A. Gross, S. Wilke, and M. Scheffler, Phys. Rev. Lett. **75**, 2718 (1995).
[3] M. Beutl, M. Riedler, and K. D. Rendulic, Chem. Phys. Lett. **247**, 249 (1995).
[4] U. Heinzmann, S. Holloway, A. W. Kleyn, R. E. Palmer, and K. J. Snowdon, J. Phys.: Condens. Matter **8**, 3245 (1996).
[5] T. Schlathölter, T. Schlathölter, M. Vicanek, and W. Heiland, J. Chem. Phys. **106**, 4723 (1997).
[6] K. Brüning, J. Granow, M. Reiniger, W. Heiland, M. Vicanek, and T. Schlathölter, Surf. Sci. **402–404**, 215 (1998).
[7] I. Wojciechowski, M. V. Medvedeva, V. K. Ferleger, K. Brüning, and W. Heiland, Nucl. Instrum. Methods Phys. Res. B **143**, 473 (1998).
[8] I. S. Bitensky and E. S. Parilis, Nucl. Instrum. Methods Phys. Res. B **2**, 364 (1984).
[9] H. Akazawa and Y. Murata, Surf. Sci. **107**, L971 (1989).
[10] T. Schlathölter, T. Schlathölter, M. Vicanek, and W. Heiland, Surf. Sci. **352–354**, 195 (1996).
[11] C. S. Sass and J. W. Rabalais, J. Chem. Phys. **89**, 3870 (1988).
[12] N. E. Henriksen, G. D. Billing, and F. Y. Hansen, Surf. Sci. **227**, 224 (1990).
[13] P. M. Echenique, F. Flores, and R. H. Ritchie, Nucl. Instrum. Methods **33**, 91 (1988).
[14] P. M. Echenique, I. Nagy, and A. Arnau, Int. J. Quantum Chem. **23**, 521 (1989).
[15] A. Närmann, H. Franke, K. Schmidt, A. Arnau, and W. Heiland, Nucl. Instrum. Methods Phys. Res. B **69**, 158 (1992).
[16] W. Tappe, A. Niehof, K. Schmidt, and W. Heiland, Europhys. Lett. **15**, 406 (1991).
[17] K. Schmidt, T. Schlathölter, A. Närmann, and W. Heiland, Chem. Phys. Lett. **200**, 465 (1992).
[18] J. K. Nørskov, Phys. Rev. B **20**, 446 (1979).
[19] B. Willerding, H. Steininger, K. J. Snowdon, and W. Heiland, Nucl. Instrum. Methods Phys. Res. B **2**, 453 (1984).
[20] H. P. Bonzel and R. Ku, J. Vac. Sci. Technol. **9**, 663 (1972).
[21] W. Heiland and E. Taglauer, Nucl. Instrum. Methods Phys. Res. B **132**, 535 (1976).
[22] R. J. MacDonald, W. Heiland, and E. Taglauer, Appl. Phys. Lett. **33**, 576 (1978).
[23] A. Närmann, H. Derks, W. Heiland, R. Monreal, E. Goldberg, and F. Flores, Surf. Sci. **217**, 255 (1989).
[24] A. Närmann, R. Monreal, P. M. Echenique, F. Flores, W. Heiland, and S. Schubert, Phys. Rev. Lett. **64**, 1601 (1990).
[25] A. Närmann, K. Schmidt, W. Heiland, R. Monreal, F. Flores, and P. M. Echenique, Nucl. Instrum. Methods Phys. Res. B **48**, 378 (1990).
[26] V. S. Remizovich, M. I. Ryazanov, and I. S. Tilinin, Sov. Phys. JETP **79**, 448 (1980).
[27] T. Schlathölter and W. Heiland, Surf. Sci. **323**, 207 (1995).
[28] K. P. Huber and G. Herzberg, *Molecular Spectra and Molecular Structure: IV. Constants of Diatomic Molecules* (Van Nostrand-Reinhold, New York, 1979).
[29] DMol (Biosym Technologies, San Diego, CA).
[30] K. Brüning, Ph.D. thesis, Universität Osnabrück, Germany, 2000.
[31] T. Schlathölter, H. Franke, M. Vicanek, and W. Heiland, Surf. Sci. **363**, 79 (1996).